

# Expression and Impact of Fibronectin, Tenascin-C, Osteopontin, and Type XIV Collagen in Fuchs Endothelial Corneal Dystrophy

Ange Tchatchouang,<sup>1-3</sup> Isabelle Brunette,<sup>4</sup> Patrick J. Rochette,<sup>1-3</sup> and Stéphanie Proulx<sup>1-3</sup>

<sup>1</sup>Centre de recherche du CHU de Québec–Université Laval, axe médecine régénératrice, Québec, Québec, Canada

<sup>2</sup>Département d'ophtalmologie et d'ORL–CCF, Faculté de médecine, Université Laval, Québec, Québec, Canada

<sup>3</sup>Centre de recherche en organogénèse expérimentale de l'Université Laval/LOEX, Québec, Québec, Canada

<sup>4</sup>Centre de recherche de l'hôpital Maisonneuve-Rosemont, Montréal, Québec, Canada

Correspondence: Stéphanie Proulx, Centre de recherche du CHU de Québec–Université Laval, Hôpital du Saint-Sacrement, 1050 chemin Ste-Foy, Québec, QC G1S 4L8, Canada;

[stephanie.proulx@fmed.ulaval.ca](mailto:stephanie.proulx@fmed.ulaval.ca).

**Received:** September 23, 2023

**Accepted:** April 2, 2024

**Published:** April 24, 2024

Citation: Tchatchouang A, Brunette I, Rochette PJ, Proulx S. Expression and impact of fibronectin, tenascin-C, osteopontin, and type XIV collagen in Fuchs endothelial corneal dystrophy. *Invest Ophthalmol Vis Sci.* 2024;65(4):38. <https://doi.org/10.1167/iovs.65.4.38>

**PURPOSE.** Fuchs endothelial corneal dystrophy (FECD) is characterized by Descemet's membrane (DM) abnormalities, namely an increased thickness and a progressive appearance of guttae and fibrillar membranes. The goal of this study was to identify abnormal extracellular matrix (ECM) proteins expressed in FECD DMs and to evaluate their impact on cell adhesion and migration.

**METHODS.** Gene expression profiles from in vitro (GSE112039) and ex vivo (GSE74123) healthy and FECD corneal endothelial cells were analyzed to identify deregulated matrix genes. Healthy and end-stage FECD DMs were fixed and analyzed for guttae size and height. Immunostaining of fibronectin, tenascin-C, osteopontin, and type XIV collagen was performed on ex vivo specimens, as well as on tissue-engineered corneal endothelium reconstructed using healthy and FECD cells. An analysis of ECM protein expression according to guttae and fibrillar membrane was performed using immunofluorescent staining and phase contrast microscopy. Finally, cell adhesion was evaluated on fibronectin, tenascin-C, and osteopontin, and cell migration was studied on fibronectin and tenascin-C.

**RESULTS.** *SPP1* (osteopontin), *FNI* (fibronectin), and *TNC* (tenascin-C) genes were upregulated in FECD ex vivo cells, and *SPP1* was upregulated in both in vitro and ex vivo FECD conditions. Osteopontin, fibronectin, tenascin-C, and type XIV collagen were expressed in FECD specimens, with differences in their location. Corneal endothelial cell adhesion was not significantly affected by fibronectin or tenascin-C but was decreased by osteopontin. The combination of fibronectin and tenascin-C significantly increased cell migration.

**CONCLUSIONS.** This study highlights new abnormal ECM components in FECD, suggests a certain chronology in their deposition, and demonstrates their impact on cell behavior.

**Keywords:** Fuchs endothelial corneal dystrophy (FECD), extracellular matrix (ECM), corneal endothelium, Descemet membrane (DM)

The cornea is the transparent tissue located at the front of the eye. The corneal endothelium, the inner layer of the cornea, plays a major role in maintaining corneal transparency by keeping the corneal stroma partially dehydrated, a process called deturgescence. When the endothelium is dysfunctional, corneal edema appears, causing corneal opacification and eventually irreversible vision loss.<sup>1,2</sup> One of the most common diseases leading to a dysfunctional endothelium is Fuchs endothelial corneal dystrophy (FECD). This endotheliopathy was responsible for 36% of the 49,110 corneal transplants reported by US eye bank members in 2021<sup>3</sup> and 41% of those performed in 10 European member states, the United Kingdom, and Switzerland.<sup>4</sup> Current treatment consists of removing the pathological endothelium

and its basal membrane (Descemet's membrane [DM]) and replacing it with that of a healthy eye bank donor cornea using surgical techniques, such as Descemet membrane endothelial keratoplasty (DMEK) or Descemet stripping automated endothelial keratoplasty (DSAEK). Recently, a new technique without transplantation has emerged, where a small central zone of DM is removed from the patient's cornea, leaving the peripheral endothelial cells to migrate and reform a functional endothelium, a technique known as Descemet stripping only (DSO) or Descemet without endothelial keratoplasty (DWEK).<sup>5</sup>

DM is continuously deposited by corneal endothelial cells (CECs) throughout their lifetime. A healthy DM contains two layers, a fetal and a postnatal layer. The stromal side of

DM is composed of type VIII collagen, type IV collagen, and fibronectin, whereas entactin, laminin, perlecan, and type IV collagen are present on its endothelial side.<sup>6</sup> The first clinical manifestation in FECD is an abnormal deposition of ECM. This leads to the formation of heterogeneously distributed excrescences on DM, called guttae, that become more numerous and wider over time.<sup>1,7</sup> DM thickness can increase up to four times the normal thickness, with two additional layers, that is, the collagenous banded layer that typically contains guttae and a loose fibrillar membrane that embeds guttae.<sup>8–10</sup> The DM composition in FECD also differs from that in healthy DM.<sup>6,9,11</sup> Previous studies have shown a higher expression of laminin, fibronectin, and type IV collagen on the endothelial side of FECD DMs compared to healthy DMs.<sup>9,11,12</sup> Type I, III, and IV collagens were also observed in the fibrillar membrane in FECD.<sup>13</sup> Normal ECM is essential to maintain tissue homeostasis, and ECM anomalies play key roles in diverse diseases.<sup>14–16</sup> Indeed, communication between cells and their ECM can impact cell migration,<sup>17</sup> adhesion,<sup>18</sup> proliferation,<sup>19</sup> and even apoptosis.<sup>20</sup> In FECD, there is evidence that guttae and the fibrillar layer alter CEC behavior and survival.<sup>13,21</sup> For instance, in cells adjacent to large guttae, the expression of  $\alpha$ SMA, n-cadherin, Snail1, and NOX4 genes was shown to be upregulated compared to cells grown on normal DMs or small guttae.<sup>21</sup> Furthermore, endothelial cell density was found to be lower in regions where the fibrillar layer is present.<sup>13</sup>

Most of the data on ECM protein expression in FECD were acquired using ex vivo tissue specimens extracted at the time of corneal transplantation.<sup>12,22–24</sup> These specimens are valuable because they represent the variability of the FECD population followed in the clinic. However, they only illustrate the end stages of the disease, and the amount of information that can be extracted from these specimens is limited, given their small size (usually 8 mm in diameter). Among the other models available to study FECD, 2D models from primary cultures<sup>10,11,19,24</sup> or from immortalized cell lines<sup>25</sup> have proven useful for gene and protein analyses and deciphering of signaling pathways. Our laboratory has also proposed a tissue-engineered 3D model produced by seeding primary cultures of FECD cells on top of decellularized corneas.<sup>11,26</sup> Using this model, we showed an early fibronectin deposition, preceding laminin and type IV collagen deposition,<sup>11</sup> whereas levels of function-related genes and proteins (pumping functionality and barrier functionality) remained similar to those of the healthy models.<sup>24</sup> Based on these results, we postulated that the tissue-engineered endothelia represented early events of FECD (prior to gutta formation) and that the early deregulation in FECD was ECM related. In the present paper, our aim was to identify other ECM proteins in late-stage ex vivo FECD specimens, as well as in earlier stage 3D models, with an aim to find a certain chronology in their deposition. We also studied the impact of some of the deregulated ECM proteins on CEC adhesion and migration.

## METHODS

All experiments were conducted in accordance with the Declaration of Helsinki. The research protocol was approved by the “Bureau de l'éthique de la recherche du CHU de Québec – Université Laval” ethics committee (DR-002-1263).

TABLE. Donor Tissue Details

	Age	Sex	Cause of Death	Figure
Healthy	82	M	Digestive hemorrhage	2
	84	F	Ruptured abdominal aortic aneurysm	2
	72	M	Neocollic	2
	73	M	Ischemic heart disease	2
	75	M	Infarction	2
	73	F	Infarction	2
	74	M	Glioblastoma	2
	68	M	Myocardial infarction	2
	63	F	Solid cancer	2
	67	M	End-stage alcoholic cirrhosis	2
	58	F	Brain glioblastoma	2,6
	80	M	Small-cell lung carcinoma	2,6,7
	59	F	Intracranial hypertension/intra parenchymal hemorrhage	4
	55	F	Ovarian neoplasia	4
	64	M	Lung cancer	4
	65	M	Multiform glioblastoma	4
	51	F	Solid cancer	4
	52	F	Breast metastatic cancer	4
	60	F	Sarcoma	4
	72	M	Infarction	6
66	F	Malignant arrhythmia	6	
82	M	Anoxic encephalopathy	6,7	
75	M	Neo urethral	7	
FECD	67	F	–	2
	73	F	–	2
	73	F	–	2
	67	M	–	2
	66	M	–	2
	75	M	–	2
	73	F	–	2
	71	M	–	3,4
	70	M	–	3,4
	86	F	–	3,4
	73	F	–	4
	74	F	–	4
	77	F	–	4
	76	M	–	4
	84	F	–	4
	85	M	–	4
	73	M	–	4,5
	73	F	–	4,5
	73	F	–	4,5
	76	F	–	5
73	F	–	5	
71	M	–	5	
74	F	–	5	
64	F	–	5	
73	M	–	5	

## Specimens

Healthy research-grade corneas (27 corneas from 23 donors) were obtained from our local eye bank (Banque d'yeux du Centre universitaire d'ophtalmologie [CUO], CHU de Québec, Québec, Québec City, Canada) with next of kin informed consent. Donor age ranged from 51 to 84 years ( $68 \pm 10$  years old; see the Table). FECD explants ( $n = 25$ ) were obtained from consenting patients with end-stage (stage 4) clinical FECD undergoing endothelial transplantation. Patient's ages ranged from 64 to 86 years ( $74 \pm 5$  years old; see the Table).

## Cell Isolation and Culture

Healthy and FECD CECs were isolated as previously described.<sup>10,27,28</sup> Briefly, DMs were peeled off and incubated overnight at 37°C in culture medium. Cells were detached from DMs using 0.02% ethylenediaminetetraacetic acid (EDTA; Millipore-Sigma, Oakville, Ontario, Canada) for 30 minutes and then the solution was aspirated up and down to dislodge the cells. Cells were seeded on FNC coating mix (Athena Enzyme Systems, Baltimore, MD, USA), as described by the manufacturer, and cultured in Opti-MEM I (Invitrogen, Burlington, Ontario, Canada) supplemented with 0.2 g/L CaCl<sub>2</sub> (Millipore-Sigma), 8% fetal bovine serum (HyClone, Logan, UT, USA), 5 ng/mL human epidermal growth factor (Austral Biologicals, San Ramon, CA, USA), 20 mg/mL ascorbic acid (Sigma-Aldrich), 0.08% chondroitin sulfate (Millipore-Sigma), and 100 IU/mL penicillin/streptomycin G (Millipore-Sigma). Cells were used between passages 3 and 6. The decellularized DMs were also collected and frozen at -20°C for subsequent analysis.

## Gene Profiling Analysis

Gene profiling data from healthy and FECD ex vivo specimens (GSE74123) and from cultured healthy and FECD cells (GSE112039) were analyzed. Matrisome genes were isolated using Array star. Matrisome genes with a linear signal higher than 100 and with a minimum of 2-fold difference between FECD and healthy specimens were kept for analysis. Heat maps were generated using GraphPad Prism version 9. The color scale reflects the log<sub>2</sub> expression level values and was obtained by the hierarchical clustering algorithm of the Euclidian metric distance between genes.

## Tissue-Engineered Corneal Endothelium

Tissue-engineered endothelia were produced as previously described.<sup>11,26,29</sup> Briefly, healthy donor corneas were devitalized by three freeze (-20°C) – thaw (4 °C) cycles and kept at -20°C until use. Dead cells on the surface of DMs were removed by rinsing. Healthy or FECD CECs were seeded on devitalized DM (100 µL cell suspension of 2.85 million cells/mL) and incubated for 3 hours before immersing the corneas in culture medium. Corneas were cultured for 14 days. Three tissue-engineered corneal endothelia, using three different cell populations, were produced per condition.

## Guttae Morphometry Analysis

Decellularized FECD DMs were fixed with 3.7% paraformaldehyde (Electron Microscopy Sciences, Hatfield, PA, USA) and counterstained with Hoechst reagent 33258 (Millipore-Sigma). Orthogonal views of DMs were obtained using a confocal microscope (Zeiss LSM-800, Toronto, Ontario, Canada) with z stacks of 20 to 35 slices of 1 µm thickness. The number of guttae on each acquisition was counted using the CellCounter plugin of ImageJ software. Guttae diameter, height, and density were analyzed using ImageJ software<sup>30</sup> and grouped by frequency distribution for statistical analysis.

## Indirect Immunofluorescence Staining and Analysis

Ex vivo and tissue-engineered endothelia were embedded in Optimal Cutting Temperature compound (Soma-gen, Edmonton, Alberta, Canada), frozen in liquid nitrogen and stored at -80°C until use. Immunofluorescence staining was performed on 20 µm-thick cryosections. Additionally, entire decellularized healthy and FECD DMs were used for en face immunostaining. All tissues were fixed with 3.7% paraformaldehyde (Electron Microscopy Sciences) for 20 minutes, permeabilized with 0.2% Triton X-100 (Fisher Scientific) for 15 minutes, and immunostained for 1 hour at room temperature using the following primary antibodies: rabbit anti-fibronectin (F14; Abcam, Toronto, Ontario, Canada), mouse anti-tenascin-C (EB2; Abcam), rabbit anti-osteopontin (8448; Abcam), and rabbit anti-type XIV collagen (NBP1; Novus Biologicals, Toronto, Ontario, Canada). After rinsing, secondary antibodies (anti-rabbit conjugated with Alexa Fluor 594 [Life Technologies, Burlington, Ontario, Canada] or anti-mouse conjugated with Alexa Fluor 488 [Life Technologies]) were incubated for 45 minutes at room temperature. Cell nuclei were counterstained with Hoechst reagent 33258 (Millipore-Sigma). Fluorescence and bright field images were obtained using a laser confocal microscope (Zeiss LSM-800, Toronto, Ontario, Canada) or an epifluorescence microscope (Zeiss Axio Imager 2, Toronto, Ontario, Canada). The mosaic function was used when the entire DM image was needed. Each immunostaining was repeated using at least three different specimens per condition.

## Adhesion Assay

Ninety-six-well plates were coated with 1 µg/cm<sup>2</sup> of fibronectin and/or tenascin-C, alone or in combination (1:1) and with 1 µg/cm<sup>2</sup> of osteopontin and/or tenascin-C, alone or in combination (1:1), for 1 hour. Wells without coating served as controls. Wells were rinsed with sterile phosphate buffered saline containing calcium and magnesium before seeding healthy CECs at a density of 30,000 cells/cm<sup>2</sup>. After 1 hour, nonadherent cells were discarded, and the wells were rinsed 3 times. Cells were fixed and permeabilized with cold 90% acetone (Fisher Scientific) at -20°C for 10 minutes. Wells were rinsed 3 more times, and cell nuclei were stained with Hoechst reagent 33258 (Millipore-Sigma) for 10 minutes. Wells were then photographed with an Eclipse TE2000 inverted microscope (Nikon, Mississauga, Ontario, Canada). Nuclei were counted using ImageJ software. Experiments were performed using three different cell populations in triplicate, and three images were acquired per well.

## Migration Assay

Wells of 12-well plates were coated with 1 µg/cm<sup>2</sup> of fibronectin and/or tenascin-C, alone or in combination (1:1). Wells without coating served as controls. The ECM protein solution was left to dry for 1 hour before a 4-chamber insert was inserted (Ibidi GmbH, Gräfelfing, Germany). Once removed, these inserts leave a uniform free area of 500 µm width. Healthy CECs were seeded at a cell density of 17,500 cells/chamber (chamber area = 0.35 cm<sup>2</sup>) until complete confluence (between 2 and 3 days), after which the inserts were removed, and cell migration was observed

using a time-lapse microscope (Axio Imager 2; Zeiss), acquiring images every 30 minutes for 24 hours. The free area was measured using ImageJ. The percentage of free area was obtained by comparing the 8 hour, 16 hour, and 24 hour acquisitions with the 0 hour acquisitions. Experiments were performed using three different cell populations.

### Statistical Analysis

The results are presented as the means of all measurements and standard deviation (SD). Statistical analyses were performed using GraphPad Prism version 9 and Microsoft Excel 2016 software (Microsoft Corp., Redmond, WA, USA). One-way or 2-way ANOVA tests were used, followed by Dunnett's multiple comparison test or a Bonferroni multiple comparison test. Any *P* value < 0.05 was considered significant.

## RESULTS

### Gene Expression of *SPP1*, *FN1*, and *TNC* Is Upregulated in FECD

To identify new abnormal ECM proteins that appear in FECD, we first analyzed the matrisome genes that were deregulated in FECD, both ex vivo (GSE74123) and in vitro (GSE112039). In FECD ex vivo specimens, 628 ECM-related genes with a mean expression linear value greater than 100 and a 2-fold deregulation were identified. Figure 1A presents the most deregulated genes coding for matrisome proteins other than matrix metalloproteinases (MMPs), tissue inhibitors of metalloproteinases (TIMPs), and glycosaminoglycans (GAGs). Of interest, *SPP1* (osteoportun), *FN1* (fibronectin), and *TNC* (tenascin-C) were upregulated 50-fold, 11-fold, and 10-fold, respectively, in ex vivo FECD. In in vitro FECD CECs, 31 ECM-

related genes with a mean linear value greater than 100 were identified, of which 18 were upregulated more than 2-fold in FECD (Fig. 1B) and 13 were downregulated, including *COL8A2* (Fig. 1C).

### Expression of Tenascin-C, Fibronectin, Osteopontin, and Type XIV Collagen in Ex Vivo Specimens and in Tissue-Engineered Models

The presence of tenascin-C, fibronectin, osteopontin, and type XIV collagen was analyzed using cross-sections of ex vivo specimens (Fig. 2). Tenascin-C, fibronectin, and osteopontin were selected following the gene profiling analysis (see Fig. 1), whereas the type XIV collagen was chosen because its gene was recently shown to be upregulated in a *SLC4A11* <sup>-/-</sup> mouse model,<sup>31</sup> and *SLC4A11* mutations were reported to be associated with FECD.<sup>31,32</sup> The results showed that all four proteins were present on the endothelial side of the DM in ex vivo FECD specimens, whereas they were absent in the healthy ex vivo specimens. Immunostaining was also performed using tissue-engineered models reconstructed using healthy and FECD cells<sup>11,24</sup> (see Fig. 2). In the FECD-engineered model, tenascin-C and fibronectin were expressed on the endothelial side of the DM, whereas osteopontin and type XIV collagen were absent. The four proteins were also absent in the healthy engineered tissue model (see Fig. 2).

### Guttae Diameter Increases in Guttae-Rich Regions of FECD DM

We performed a morphometric analysis of guttae using orthogonal views of DMs obtained by confocal microscopy to determine how their diameter and height evolved according to their density (Fig. 3A). Guttae density varied from

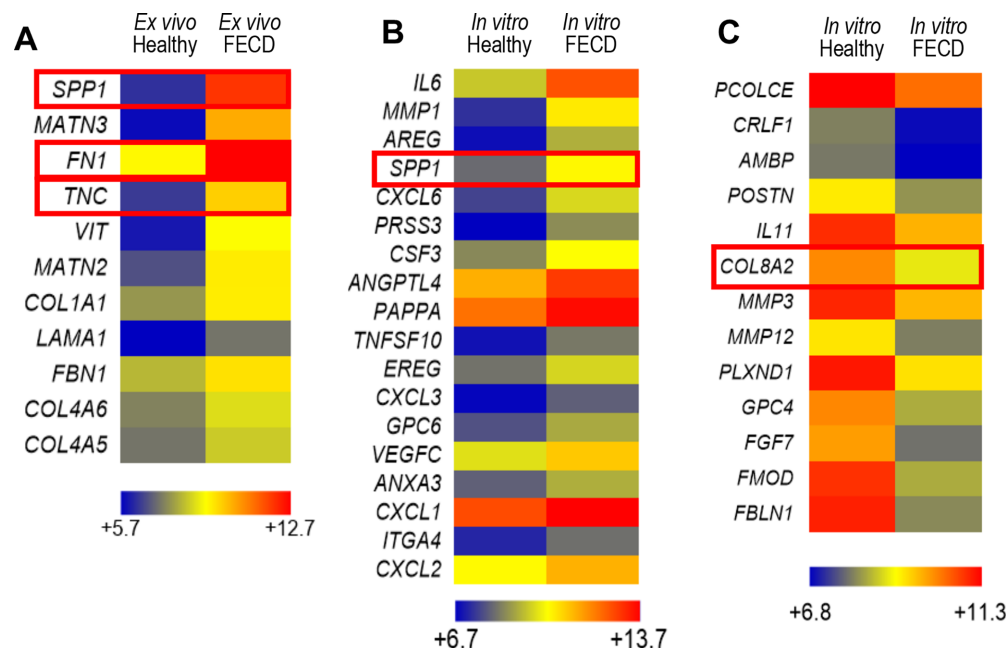
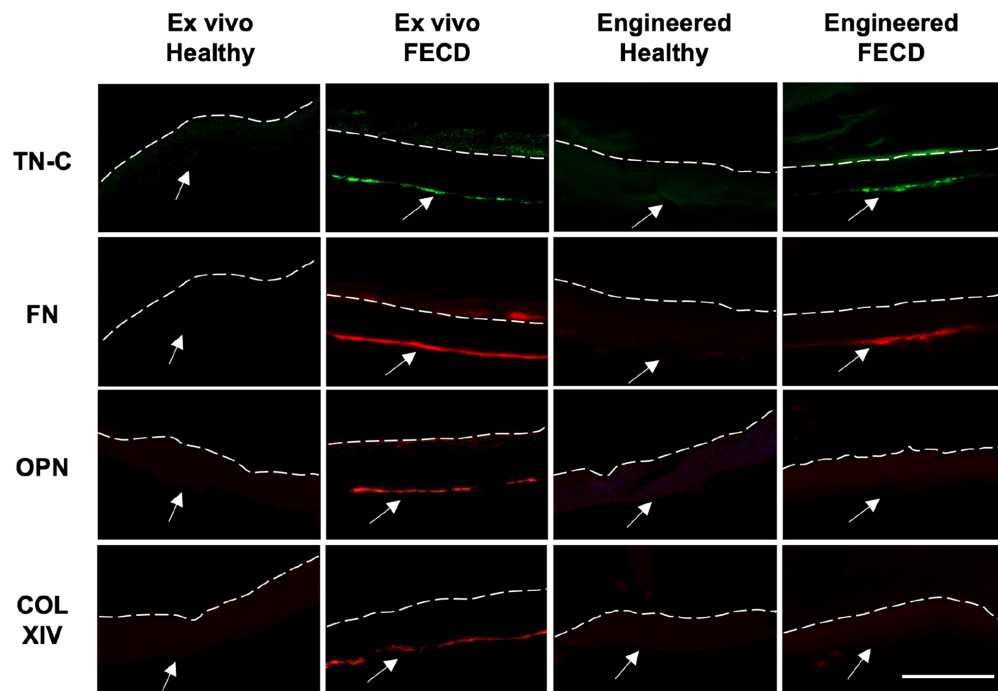


FIGURE 1. Heatmaps of matrisome-related genes in healthy and FECD cells. The most deregulated ex vivo (A) and in vitro (B, C) matrisome-related genes in healthy and FECD cell populations. Red rectangles indicate genes of interest.



**FIGURE 2.** Expression of extracellular matrix proteins in ex vivo and tissue-engineered healthy and FECD conditions. Immunostaining of tenascin-C (TN-C; *green*), fibronectin (FN; *red*), osteopontin (OPN; *red*), and type XIV collagen (COL XIV; *red*) on cross sections of healthy and FECD ex vivo tissues and on corneal endothelia engineered using healthy and FECD cells. The *white dashed line* indicates the stromal side of the Descemet membrane. The *white arrow* shows the endothelial side of the Descemet membrane. The results are representative of three different specimens per condition. TN-C and FN immunostaining were performed on the same specimens. Scale bar = 50  $\mu$ m.

0 in the periphery of the specimens to 1328 guttae/ $\text{mm}^2$  in the center of the specimens (Figs. 3B, 3D). Guttae density was categorized using the grouped frequency distribution method. The results showed a statistically significant increase in guttae diameter from  $11 \pm 3 \mu\text{m}$  for densities between 30 and 330 guttae/ $\text{mm}^2$  to  $14 \pm 5 \mu\text{m}$  for 630 guttae/ $\text{mm}^2$  and over (Fig. 3C). Fluctuations in mean guttae height, between  $8 \pm 1 \mu\text{m}$  and  $9 \pm 2 \mu\text{m}$ , were not significant, regardless of guttae distribution (Fig. 3E). This analysis allowed us to define guttae-rich regions as those with more than 630 guttae/ $\text{mm}^2$  and guttae-poor regions as those with less than 330 guttae/ $\text{mm}^2$ .

#### Tenascin-C, Fibronectin, and Osteopontin Are Expressed in Guttae-Rich Areas of FECD DM

The link between ECM expression and guttae density was evaluated using en face immunostaining (Fig. 4A). Tenascin-C was clearly expressed in guttae-rich regions, faintly expressed in guttae-poor regions, and was also present in areas with no gutta. Fibronectin was expressed across the entire DM. Osteopontin was mostly expressed in guttae-rich areas, and its expression was more diffuse. Type XIV collagen was absent in no-gutta and guttae-poor areas and was expressed in guttae-rich areas, mostly concentrated at the periphery of guttae. In guttae-rich regions, orthogonal views allowed us to observe that tenascin-C, fibronectin, and osteopontin proteins covered guttae and DM, whereas type XIV collagen was present on the side of guttae (Fig. 4B).

#### Tenascin-C, Fibronectin, and Osteopontin Are Expressed in the Fibrillar Layer of the FECD DM

In the late stages of FECD, a fourth layer, the fibrillar layer, is formed over the DM in guttae-rich regions, surrounding and embedding guttae.<sup>10</sup> Using brightfield imaging, the fibrillar layer is visible as fibrillar-like structures, and the guttae are less visible when buried underneath. By selecting these fibrillar-like regions (Fig. 5 second column), we were able to study the relationship between the presence of a fibrillar layer and ECM protein expression (see Fig. 5). The results showed that tenascin-C and osteopontin were present in the fibrillar layer-like structures, whereas fibronectin was expressed in and outside the fibrillar layer-like structure. Type XVI collagen was mostly present outside the regions of the fibrillar-like membrane structures.

#### Tenascin-C Does not Prevent Corneal Endothelial Cells From adhering to Fibronectin, and Osteopontin Decreases Cell Adhesion

Because there is a progressive decrease in cell density in FECD,<sup>33</sup> we assessed whether tenascin-C could interfere with CEC adhesion to fibronectin, as observed in other diseases,<sup>34</sup> which could lead to cell detachment and explain cell loss. CEC adhesion on fibronectin remained similar to that of the control (Fig. 6A), regardless of the different coating protein concentration used (Supplementary Fig. S1). Compared to uncoated plates, there was a small decrease in the number of cells that adhered to  $1 \mu\text{g}/\text{cm}^2$  tenascin-C-coated wells (from

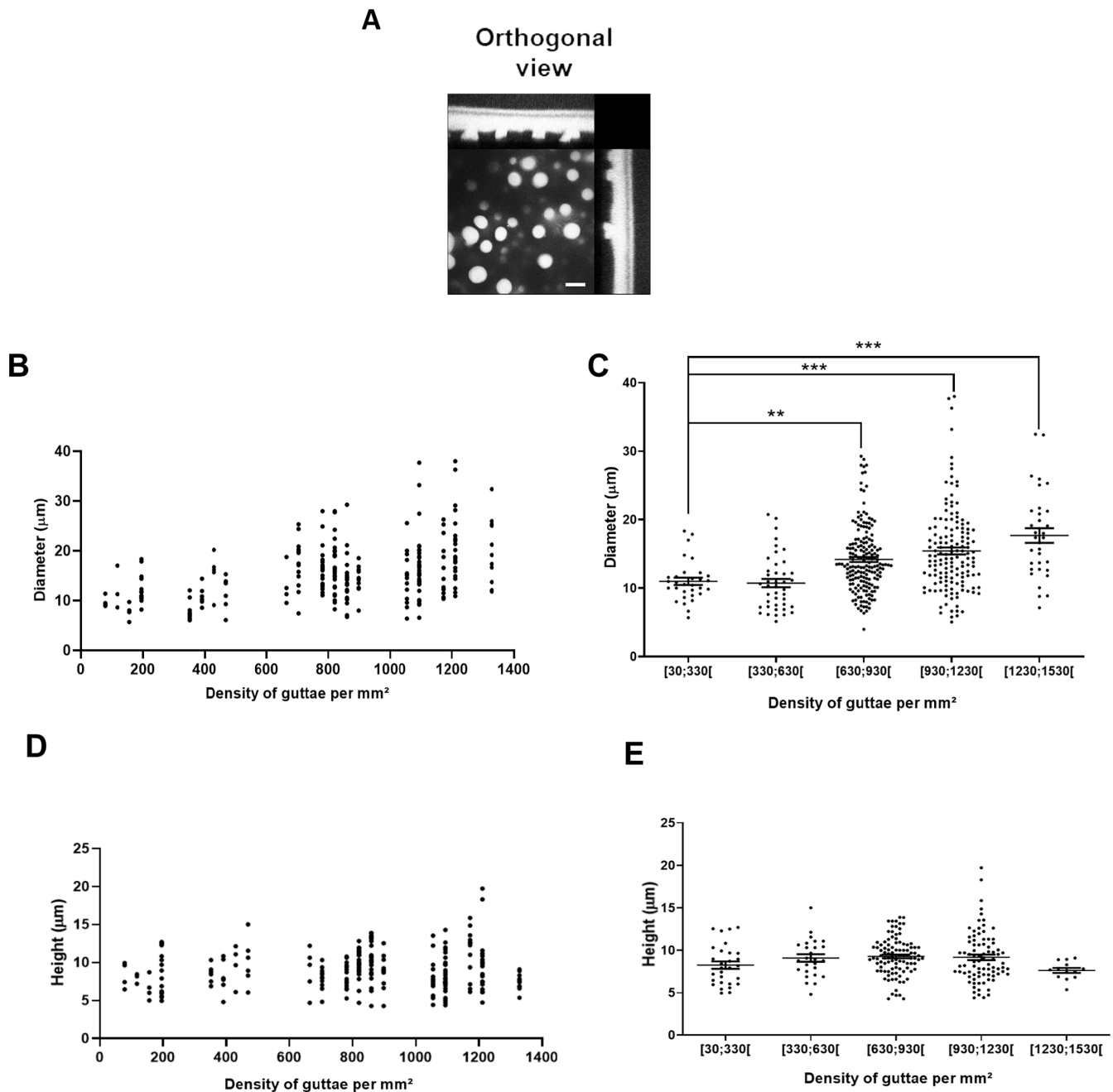


**FIGURE 3.** Association among guttae diameter, height, and density. (A) Orthogonal view of a DM used for guttae diameter, height, and density analysis. Scale bar = 20 µm. (B) Guttae diameter according to guttae density. (C) Guttae diameter distributed in classes of guttae density per mm<sup>2</sup>. (D) Guttae height according to guttae density. (E) Guttae height distributed in classes of guttae density per mm<sup>2</sup>. Each dot represents a single guttae. The results from three different FECD specimens are presented on the same graph. \*\**P* < 0.001; \*\*\**P* < 0.0001.

2172 ± 472 to 1852 ± 442 adherent cells). This decrease was not statistically significant. There were no statistically significant differences between adhesion on fibronectin and adhesion on fibronectin/tenascin-C co-coating. We also assessed CEC adhesion to osteopontin. The results showed a statistically significant decrease in the number of adhered cells on osteopontin (from 5360 ± 425 on uncoated wells to 4363 ± 413 on osteopontin), although the adhesion rate to tenascin-C and to the osteopontin/tenascin-C co-coating (1:1) was similar to that of the control (Fig. 6B).

### The Combination of Tenascin-C and Fibronectin Increases Corneal Endothelial Cell Migration

The ECM can also influence cell migration.<sup>17</sup> Healthy CEC migration on tenascin-C and/or fibronectin was followed using a migration assay and time-lapse microscopy (Figs. 6C, 6D). After 24 hours, fibronectin alone increased CEC migration by 19.4% over the control. Tenascin-C alone showed similar migration compared to controls but decreased migration by 26.2% compared to fibronectin. The combination

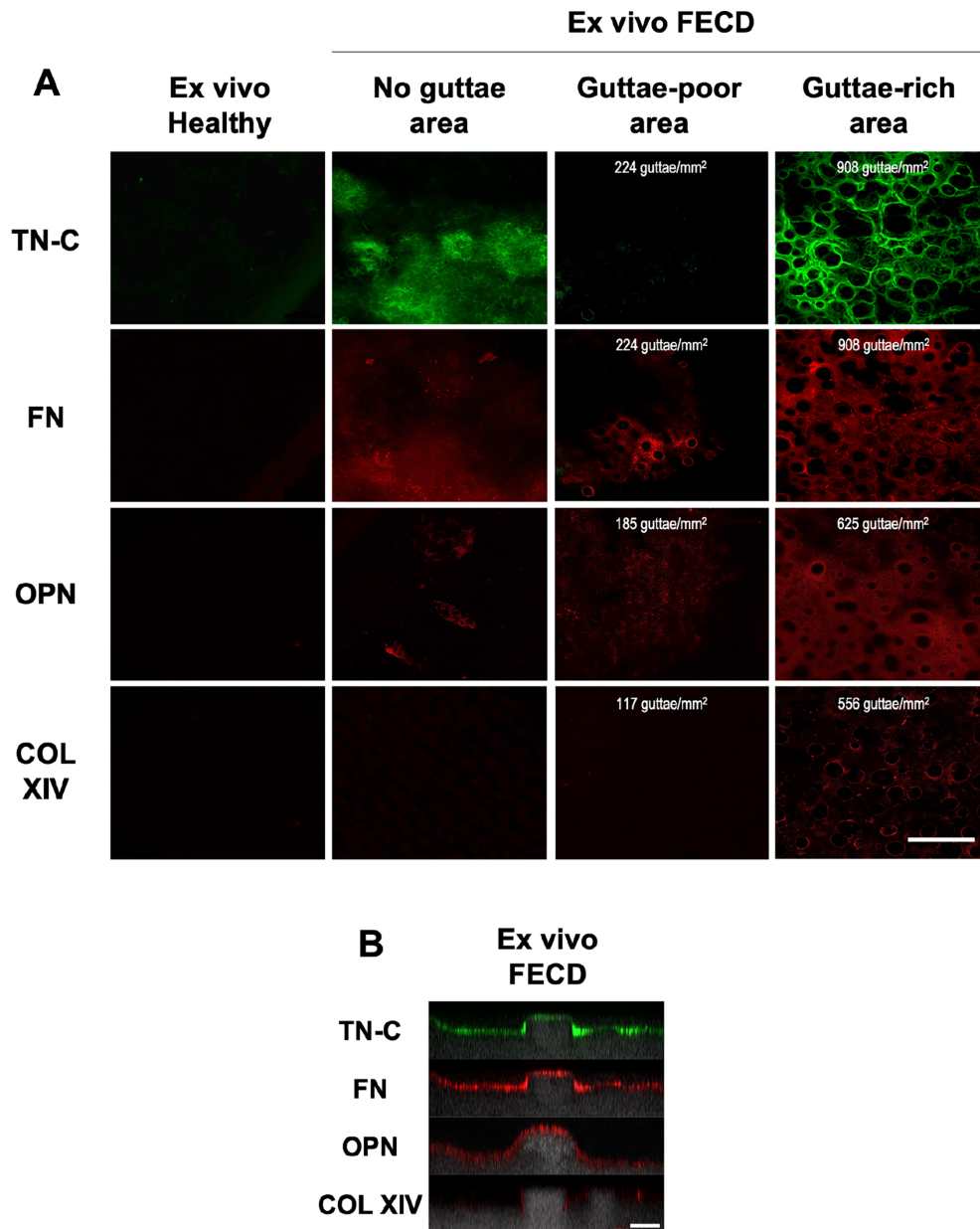


**FIGURE 4.** Localization of extracellular matrix proteins of different regions of ex vivo DM. En face view (A) and orthogonal view (B) immunostaining of tenascin-C (TN-C; green), fibronectin (FN; red), osteopontin (OPN; red), and type XIV collagen (COL XIV; red) in healthy and FECD ex vivo tissues. The results are representative of at least three different specimens per condition. TN-C and FN immunostaining were performed on the same specimens. Scale bars = 100  $\mu$ m (A) and 20  $\mu$ m (B).

of tenascin-C and fibronectin increased cell migration by 31.2% over controls; the scratch was completely closed at 24 hours.

### DISCUSSION

Thickening of DM, formation of guttae, and end-stage deposition of a fibrillar membrane are chronological hallmarks of FECD. In this study, we identified new abnormal ECM proteins that are expressed in FECD DMs, namely, osteopontin, and type XIV collagen. We show that tenascin-C and osteopontin are strongly expressed in the fibrillar membrane regions, fibronectin is expressed throughout FECD DMs, and

type XIV collagen is exclusively present on the sides of guttae. Furthermore, we demonstrate that tenascin-C does not interfere with the adhesion of cells to fibronectin at the protein coating concentrations tested, and that the combination of fibronectin and tenascin-C increases cell migration. In parallel, an in-depth morphometric analysis of guttae revealed that once they reached a density of 630 guttae/mm<sup>2</sup>, guttae diameter continued to increase, whereas their height remained stable.

ECM gene deregulation in late-stage FECD specimens has been previously studied.<sup>12,35</sup> Weller et al. identified several collagen genes (*COLIV*, *COLIA1*, and *COL3A1*), glycoproteins (*FN1* and *LAMA2*), integrins (*ITGA1*, *ITGA3*, *ITGA4*, *ITGB1*, and *ITGB3*), metalloproteinases and their inhibitors

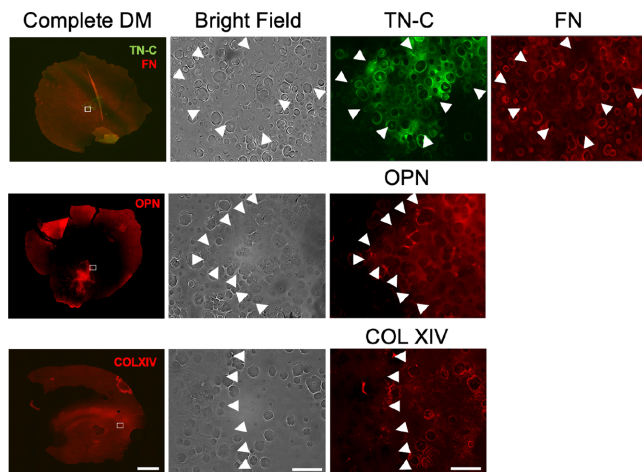


**FIGURE 5.** Expression of extracellular matrix proteins with reference to the fibrillar layer of FECD DM. *First column:* Mosaic of the entire FECD Descemet membrane (DM) at low (5X) magnification immunostained against ECM proteins (*first row:* tenascin-C [TN-C; green] and fibronectin [FN; red] co-immunostaining; *second row:* osteopontin [OPN; red]; and *third row:* type XIV collagen [COL XIV; red]). *White squares* represent the regions that are presented in the higher magnifications (20X) of the second, third and fourth columns. Scale bar = 2 mm. *Second column:* Brightfield images. *Arrowheads* point to the fibrillar-like regions of FECD DM. Scale bar = 100  $\mu$ m. *Third and fourth columns* are ECM immunostainings (*first row:* tenascin-C [green] and fibronectin [red] coimmunostaining; *second row:* osteopontin [red]; and *third row:* type XIV collagen [red]). *Arrowheads* point to the fibrillar-like regions of FECD DM. Scale bar = 100  $\mu$ m. The results are representative of three different specimens per condition. TN-C and FN immunostaining were performed on the same specimens.

(*MMP10*, *MMP14*, and *TIMP1*), and apolipoproteins (*CLU*) as upregulated in FECD specimens. The protein expression of some of them, such as clusterin and type III collagen, has been confirmed on FECD DMs.<sup>12</sup> Matthaai et al. reported increased gene expression of *FN*, *LAMC1*, *COL1A1*, and *COL3A1* and demonstrated that their upregulation was followed by an abnormal deposition of the proteins encoded by these genes.<sup>35</sup> Cui et al. observed an upregulation of *FN1* and *TNC* genes in FECD ex vivo specimens,<sup>36</sup> and a recent transcriptome analysis identified *FN1*, *SPP1*, and *COL6A2* as the top upregulated genes in FECD ex vivo specimens.<sup>37</sup> Herein, we confirmed the upregulation of *FN1*, *TNC*, and *SPP1* in FECD.

Tenascin-C was selected for protein analysis because of its role in modulating cell adhesion and migration to fibronectin,<sup>38,39</sup> an ECM protein clearly present in FECD DMs.<sup>9,11</sup> Tenascin-C is a glycoprotein expressed in the epithelial basement membrane and the anterior corneal stroma of FECD specimens,<sup>40</sup> and its presence in FECD DMs has recently been demonstrated.<sup>41</sup> The upregulation of the *SPP1* gene raised interest because it was the only ECM-related gene overexpressed both ex vivo and in vitro in FECD CECs. Its protein, osteopontin, is a matrix structural glycoposphoprotein that acts as a cytokine and regulates the activity of resident tissue cells at sites of injury. Interestingly, both tenascin-C and osteopontin are ligands for the integrin  $\alpha$ 9 subunit, the gene for which is upregulated in FECD (GSE74123). Both proteins are known for their role in wound healing.<sup>42,43</sup> Osteopontin is also a master regulator of endothelial to mesenchymal transition (EMT),<sup>44</sup> a process

that has been proposed to be implicated in FECD pathogenesis.<sup>25,45</sup> The *COLXIV* gene encodes a FACIT collagen that binds fibrillar collagens, which are the main components of DM. It was selected due to its major upregulation in an *SLC4A11*-deficient mouse.<sup>31</sup> The *SLC4A11* gene encodes a member of the SLC4 family of bicarbonate transport proteins that contributes to osmotically maintaining corneal fluid balance. Its downregulation is known to be one of the genetic causes of FECD.<sup>33,46,47</sup> Surprisingly, the *COLXIV* gene was not upregulated in the gene profiling of ex vivo (GSE74123) and in vitro (GSE112039) FECD cells. Perhaps the specimens used for the transcriptome analysis came from patients who did not carry an *SLC4A11* mutation, although this remains to be confirmed. Interestingly, in addition to identifying new upregulated aberrant ECM genes, our in vitro analysis showed downregulation of the *COLVIII* gene. Its protein, type VIII collagen, is the major constituent of DM. The decrease in healthy ECM might also contribute to the diseased DM environment.

Guttae apparition is one of the first clinical signs of the disease. They typically first appear centrally and slowly continue to expand toward the periphery.<sup>1,7</sup> Clinically, slit-lamp grading of guttae density is used to judge the severity of the disease. According to the Krachmer grading scale for FECD, the presence of more than 12 central nonconfluent guttae corresponds to a severity grade of 1, and the presence of more than 5 mm confluent guttae corresponds to a severity grade of 4.<sup>48</sup> It is still unclear why guttae first appear and increase in density in the center of the cornea. A partial explanation might be that the central cornea is more exposed to UV light<sup>49</sup> and that UV exposure induces oxidative stress,<sup>50</sup> which was demonstrated to be more severe in the center.<sup>51</sup> Because FECD CECs are more sensitive to oxidative stress,<sup>52</sup> central CECs would be the first to be affected by the disease, explaining why guttae are more numerous in the center of DM. A greater guttae density is associated with a greater CEC loss,<sup>1,2</sup> and it is now acknowledged that guttae can alter CEC survival according to their diameter.<sup>21</sup> In this study, we confirmed that guttae were larger where their distribution was denser. It is interesting to note that although guttae become wider with time, their height remains stable. The fact that CECs cannot cover large guttae<sup>21</sup> and the possibility that they continue to deposit ECM on the side of the guttae explains why guttae become wider but not taller.

Immunostaining of late-stage FECD ex vivo specimens was performed to establish a possible relationship among the four proteins of interest (fibronectin, tenascin-C, osteopontin, and type IV collagen) and guttae density. As reported, fibronectin was expressed on FECD DMs.<sup>9,11,12</sup> Fibronectin and tenascin-C were mostly present in the fibrillar membrane layer in guttae-rich regions but also regions without guttae. Type XIV collagen was only present around guttae in guttae-rich regions. Osteopontin was located in the fibrillar layer in guttae-rich regions. Given that the fibrillar membrane appears in later stages, its presence could therefore represent a more advanced stage of the disease, and, inversely, regions without guttae might represent an earlier stage of the disease. The immunostainings of these specimens suggest that chronologically, fibronectin and tenascin-C are first deposited, then guttae forms and type XIV collagen is deposited around them when guttae reach high density, followed by the formation of a fibrillar membrane that embeds guttae in a



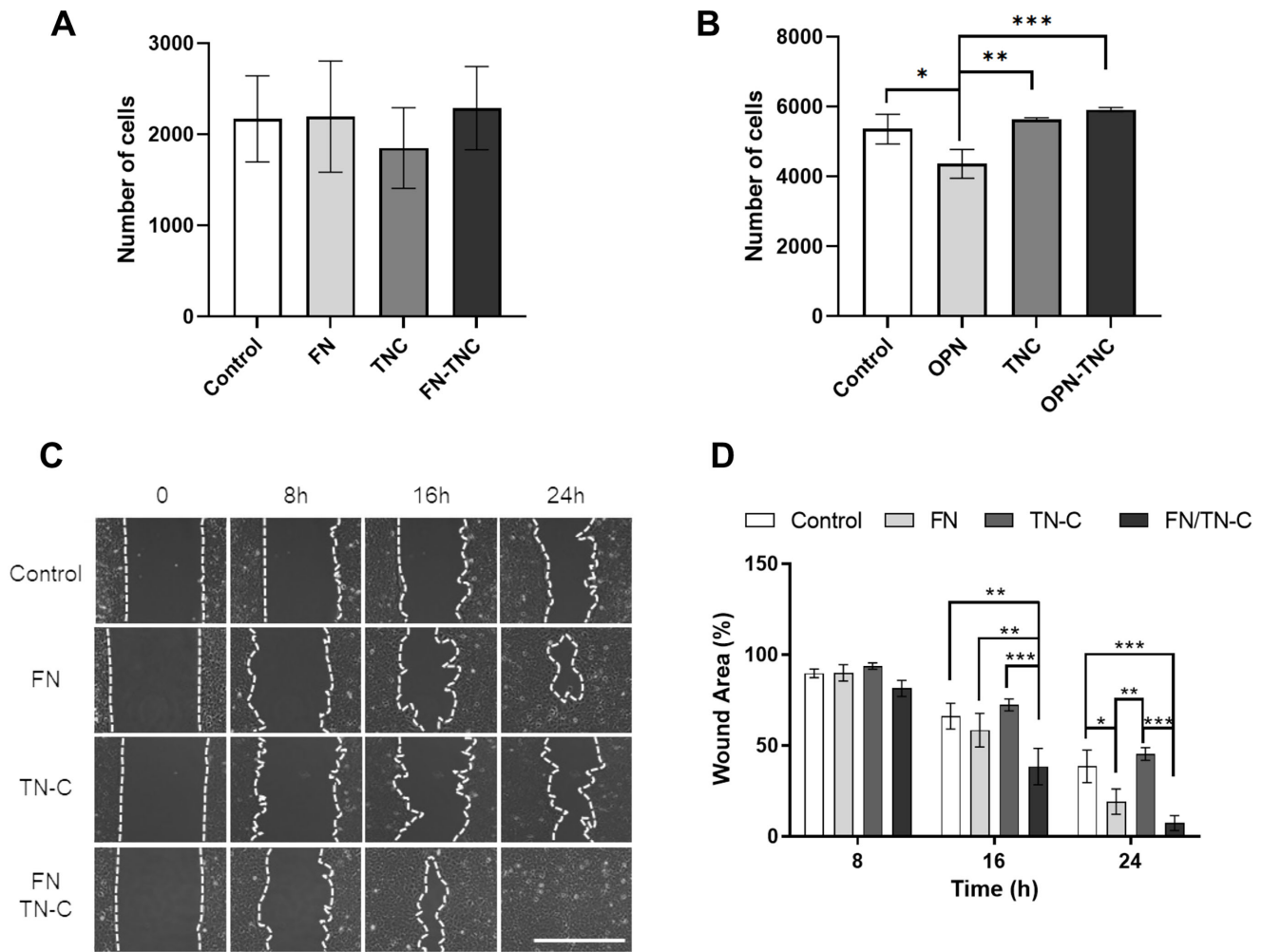


**FIGURE 6.** Impact of extracellular matrix on cell adhesion and migration. (A, B) Adhesion assays were performed on fibronectin (FN) and tenascin-C (TNC) (A) and on osteopontin (OPN) and TNC (B). The number of adherent cells was quantified after 1 hour. (C) Migration assays with 1000 ng/cm<sup>2</sup> fibronectin (FN), tenascin-C (TN-C), and the combination of fibronectin and tenascin-C (FN/TN-C) were performed for 24 hours. White dotted lines indicate the wound edges. (D) Quantification of the scratch areas at 8 hours, 16 hours, and 24 hours compared to 0 hours. \**P* < 0.05; \*\**P* < 0.01; \*\*\**P* < 0.001.

fibrous layer composed of tenascin-C, osteopontin, and fibronectin.

In contrast to late-stage FECD ex vivo specimens in which the disease has progressed for approximately 50 years, tissue-engineered FECD models allow the study of proteins that are rapidly deregulated in vitro and before the appearance of guttae.<sup>11,24</sup> Combined with the ex vivo data, the tissue-engineered FECD model allows to add elements of information regarding the timeline of ECM deregulations, where the in vitro model would be the first deregulations, followed by the periphery of ex vivo specimens where there are few guttae, followed by the guttae-rich regions at the center of the ex vivo specimens, where the disease is most advanced. It makes sense that the tissue-engineered models did not express osteopontin or type IV collagen, as these two ECM proteins were observed only ex vivo after the appearance of guttae. Accordingly, fibronectin and tenascin-C were observed in the tissue-engineered FECD model, and they were also expressed ex vivo in regions without guttae. Thus, the tissue-engineered models seem to recapitulate the chronology of ECM deposition suggested with the ex vivo

specimens, with an early accumulation of fibronectin and tenascin-C.

It is also interesting to note that fibronectin and tenascin-C are not only produced in the early stages of the disease but also seem to be continuously produced by FECD CECs throughout the disease, because they are expressed in all regions of the FECD DM (no gutta, guttae-rich, and fibrillar membrane). Their accumulation could also mean a lack of degradation. Indeed, previous findings highlighted an imbalance in MMP expression in FECD, where MMP2 and MMP10 expression decreased in cultured FECD CECs. MMP2 and MMP10 are known to degrade fibronectin<sup>53</sup>; therefore, their downregulation could explain the accumulation of this ECM protein. It has also been shown that the *MMP14*, *MMP9*, and *MMP3* genes were downregulated in FECD ex vivo cells.<sup>54</sup> *MMP14* is known to cleave fibronectin,<sup>55</sup> *MMP9* cleaves tenascin-C<sup>56</sup> and osteopontin is a ligand of *MMP3*.<sup>57</sup> Thus, it could be postulated that this decrease in MMPs prevents the degradation of tenascin-C, fibronectin, and osteopontin by CECs during disease progression.

After 1 hour of attachment and thorough rinsing, a similar number of cells remained in the wells covered with fibronectin and tenascin-C, alone or in combination, demonstrating that tenascin-C does not interfere with the ability of CECs to adhere to fibronectin, confirming previous results.<sup>58</sup> Our results also demonstrated that osteopontin decreased CEC adhesion compared to the control, tenascin-C, and the combination osteopontin/tenascin-C. As osteopontin is known to be a protein that promotes cell adhesion,<sup>59</sup> our results suggest that adhesive forces may be weaker on osteopontin compared to tenascin-C. Indeed, weak adhesive forces could explain cell detachment following rinsing. The necessity of additional adhesive forces following the first signs of attachment and the influence of different ECM proteins on this attachment have been previously demonstrated by Engler et al.<sup>60</sup>

Fibronectin also increased cell migration, which was even more marked when CECs migrated on a combination of both tenascin-C and fibronectin. These results were particularly noteworthy because, to our knowledge, the combined role of these two glycoproteins on CECs has not yet been studied. The presence of fibronectin and tenascin-C throughout the disease thus suggests an increase in cell migration, perhaps in an attempt to maintain endothelial monolayer integrity despite cell losses in the early phases of the disease,<sup>33</sup> and/or maybe in an attempt to navigate around guttae in later stages of the disease, as guttae were shown to decrease cell migration.<sup>61</sup> On the other hand, the aberrant expression of fibronectin, tenascin-C, and osteopontin in the fibrillar membrane may contribute to cell death. Indeed, excessive accumulation of ECM changes tissue homeostasis, which can lead to pathological phenotypes.<sup>15,62,63</sup> Moreover, Hribek et al. highlighted that the fibrillar membrane might be a toxic environment for CECs, which are less dense in this region.<sup>13</sup>

FECD is a multifactorial disease, and variability from one patient to another is high. Indeed, FECD etiology remains difficult to establish. Herein, we present new knowledge about FECD ECM, when these ECM proteins probably appear, and how they could impact corneal endothelial cell behavior. We identified two ECM proteins, fibronectin and tenascin-C, that could become useful markers for in vitro pharmacological studies aimed at controlling ECM deposition to slow FECD pathogenesis using in vitro models. From a clinical point of view, our results highlight the importance of removing the region of DM where the fibrillar layer is present to optimize the success of Descemet stripping only (DSO) surgery for patients with FECD.

### Acknowledgments

The authors would like to thank Mathieu Thériault, Gaëtan LeBel and Simon Jacob for technical assistance, as well as the coordinators of the Ocular research tissues infrastructure for their help in ocular tissue distribution. The authors would also like to thank the corneal surgeons, the operating room nurses, as well as the eye bank personal for their ongoing collaboration in obtaining FECD specimens: Patricia-Ann Laughrea, Richard Bazin, Marie Eve Légaré, Mathieu Mercier, and Ralph Kyrillos from the Centre Universitaire d'ophtalmologie (CUO) du CHU de Québec (CUO-CHU de Québec), Isabelle Brunette, Johanna Choremis, Julia Talajic, and Tanguy Boutin from the CUO de l'Université de Montréal à l'hôpital Maisonneuve-Rosemont (CUO-HMR). A.T. received a travel grant from the Vision Health Research Network and the Cell, Tissue, and Gene Therapy Network. I.B. is the director of the Regenerative Medicine and Translational Research Program funded of the Suzanne Véron-

neau Trautman Chair, Université de Montréal, Canada. S.P. and P.J.R. are research scholars from the FRQ-S.

Supported by the Canadian Institute for Health Research (I.B., P.J.R., and S.P.). Procurement of eyes and corneas for research from the CUO Eye bank was possible thanks to an infrastructure from the Vision Health Research Network (S.P.), a network supported by the Fonds de recherche du Québec – Santé (FRQ-S).

Disclosure: **A. Tchatchouang**, None; **I. Brunette**, None; **P.J. Rochette**, None; **S. Proulx**, None

### References

1. Adamis AP, Filatov V, Tripathi BJ, Tripathi RC. Fuchs' endothelial dystrophy of the cornea. *Surv Ophthalmol*. 1993;38(2):149–168.
2. Elhalis H, Azizi B, Jurkunas UV. Fuchs endothelial corneal dystrophy. *Ocul Surf*. 2010;8(4):173–184.
3. 2021\_Statistical report EBAA.pdf.
4. Dunker SL, Armitage WJ, Armitage M, et al. Practice patterns of corneal transplantation in Europe: first report by the European Cornea and Cell Transplantation Registry. *J Cataract Refract Surg*. 2021;47(7):865–869.
5. Khan NC, Lin CC. Descemet stripping only for Descemet's membrane detachment and sectoral corneal edema. *Am J Ophthalmol Case Rep*. 2022;29:101784.
6. Kabosova A, Azar DT, Bannikov GA, et al. Compositional differences between infant and adult human corneal basement membranes. *Invest Ophthalmol Vis Sci*. 2007;48(11):4989–4999.
7. Zhang J, Patel DV. The pathophysiology of Fuchs' endothelial dystrophy – a review of molecular and cellular insights. *Exp Eye Res*. 2015;130:97–105.
8. Yuen HKL, Rassier CE, Jardeleza MSR, et al. A morphologic study of Fuchs dystrophy and bullous keratopathy. *Cornea*. 2005;24(3):319–327.
9. Gottsch JD, Zhang C, Sundin OH, Bell WR, Stark WJ, Green WR. Fuchs corneal dystrophy: aberrant collagen distribution in an L450W mutant of the COL8A2 gene. *Invest Ophthalmol Vis Sci*. 2005;46(12):4504–4511.
10. Zaniolo K, Bostan C, Rochette Drouin O, et al. Culture of human corneal endothelial cells isolated from corneas with Fuchs endothelial corneal dystrophy. *Exp Eye Res*. 2012;94(1):22–31.
11. Goyer B, Thériault M, Gendron SP, Brunette I, Rochette PJ, Proulx S. Extracellular matrix and integrin expression profiles in Fuchs endothelial corneal dystrophy cells and tissue model. *Tissue Eng Part A*. 2018;24(7-8):607–615.
12. Weller JM, Zenkel M, Schlötzer-Schrehardt U, Bachmann BO, Tourtas T, Kruse FE. Extracellular matrix alterations in late-onset Fuchs' corneal dystrophy. *Invest Ophthalmol Vis Sci*. 2014;55(6):3700–3708.
13. Hribek A, Clahsen T, Horstmann J, et al. Fibrillar layer as a marker for areas of pronounced corneal endothelial cell loss in advanced Fuchs endothelial corneal dystrophy. *Am J Ophthalmol*. 2021;222:292–301.
14. Hahn K, Sundar IK. Current perspective on the role of the circadian clock and extracellular matrix in chronic lung diseases. *Int J Environ Res Public Health*. 2023;20(3):2455.
15. Sloniecka M, Danielson P. Acetylcholine decreases formation of myofibroblasts and excessive extracellular matrix production in an in vitro human corneal fibrosis model. *J Cell Mol Med*. 2020;24(8):4850–4862.
16. Brown Y, Hua S, Tanwar PS. Extracellular matrix in high-grade serous ovarian cancer: advances in understanding of

- carcinogenesis and cancer biology. *Matrix Biol.* Published online February 11, 2023.
17. Yamada KM, Collins JW, Cruz Walma DA, et al. Extracellular matrix dynamics in cell migration, invasion and tissue morphogenesis. *Int J Exp Pathol.* 2019;100(3):144–152.
  18. Hidalgo-Bastida LA, Cartmell SH. Mesenchymal stem cells, osteoblasts and extracellular matrix proteins: enhancing cell adhesion and differentiation for bone tissue engineering. *Tissue Eng Part B Rev.* 2010;16(4):405–412.
  19. Xu Z, Orkwis JA, DeVine BM, Harris GM. Extracellular matrix cues modulate Schwann cell morphology, proliferation, and protein expression. *J Tissue Eng Regen Med.* 2020;14(2):229–242.
  20. Adams CS, Shapiro IM. Mechanisms by which extracellular matrix components induce osteoblast apoptosis. *Connect Tissue Res.* 2003;44(1):230–239.
  21. Kocaba V, Katikireddy KR, Gipson I, Price MO, Price FW, Jurkunas UV. Association of the gutta-induced microenvironment with corneal endothelial cell behavior and demise in Fuchs endothelial corneal dystrophy. *JAMA Ophthalmol.* 2018;136(8):886–892.
  22. Hu J, Rong Z, Gong X, et al. Oligonucleotides targeting TCF4 triplet repeat expansion inhibit RNA foci and mis-splicing in Fuchs' dystrophy. *Hum Mol Genet.* 2018;27(6):1015–1026.
  23. Kelliher C, Chakravarti S, Vij N, et al. A cellular model for the investigation of Fuchs' endothelial corneal dystrophy. *Exp Eye Res.* 2011;93(6):880–888.
  24. Thériault M, Gendron SP, Brunette I, Rochette PJ, Proulx S. Function-related protein expression in Fuchs endothelial corneal dystrophy cells and tissue models. *Am J Pathol.* 2018;188(7):1703–1712.
  25. Okumura N, Minamiyama R, Ho LT, et al. Involvement of ZEB1 and Snail1 in excessive production of extracellular matrix in Fuchs endothelial corneal dystrophy. *Lab Invest.* 2015;95(11):1291–1304.
  26. Haydari MN, Perron MC, Laprise S, et al. A short-term in vivo experimental model for Fuchs endothelial corneal dystrophy. *Invest Ophthalmol Vis Sci.* 2012;53(10):6343–6354.
  27. Zhu C, Joyce NC. Proliferative response of corneal endothelial cells from young and older donors. *Invest Ophthalmol Vis Sci.* 2004;45(6):1743–1751.
  28. Santerre K, Proulx S. Isolation efficiency of collagenase and EDTA for the culture of corneal endothelial cells. *Mol Vis.* 2022;28:331–339.
  29. Proulx S, Audet C, Uwamaliya Jd'Arc, et al. Tissue engineering of feline corneal endothelium using a devitalized human cornea as carrier. *Tissue Eng Part A.* 2009;15(7):1709–1718.
  30. Rasband W. ImageJ, U.S. National Institutes of Health, Bethesda, Maryland, USA. In: 2011. Accessed July 2, 2023. Available at: <https://www.semanticscholar.org/paper/ImageJ,-U.S.-National-Institutes-of-Health,-USA-Rasband/034dbc2e4c735500c519183180f8cf6033fcb28d>.
  31. Alvarez BV, Piché M, Aizouki C, et al. Altered gene expression in slc4a11<sup>-/-</sup> mouse cornea highlights SLC4A11 roles. *Sci Rep.* 2021;11:20885.
  32. Tsedilina TR, Sharova E, Iakovets V, Skorodumova LO. Systematic review of SLC4A11, ZEB1, LOXHD1, and AGBL1 variants in the development of Fuchs' endothelial corneal dystrophy. *Front Med.* 2023;10:1153122.
  33. Eghrari AO, Riazuddin SA, Gottsch JD. Chapter Seven - Fuchs Corneal Dystrophy. In: Hejtmancik JF, Nickerson JM, eds. *Progress in Molecular Biology and Translational Science.* Vol 134. Molecular Biology of Eye Disease. Cambridge, MA: Academic Press; 2015:79–97.
  34. Paron I, Berchtold S, Vörös J, et al. Tenascin-C enhances pancreatic cancer cell growth and motility and affects cell adhesion through activation of the integrin pathway. *PLoS One.* 2011;6(6):1–9.
  35. Matthaer M, Leitl C, Cursiefen C, Heindl LM. Correlation of extracellular matrix-related gene expression with objective Fuchs endothelial corneal dystrophy severity. *Clin Experiment Ophthalmol.* 2019;47(5):671–673.
  36. Cui Z, Zeng Q, Guo Y, et al. Pathological molecular mechanism of symptomatic late-onset Fuchs endothelial corneal dystrophy by bioinformatic analysis. *PLoS One.* 2018;13(5):e0197750.
  37. Nakagawa T, Tokuda Y, Nakano M, et al. RNA-Seq-based transcriptome analysis of corneal endothelial cells derived from patients with Fuchs endothelial corneal dystrophy. *Sci Rep.* 2023;13:8647.
  38. Fiorilli P, Partridge D, Staniszevska I, et al. Integrins mediate adhesion of medulloblastoma cells to tenascin and activate pathways associated with survival and proliferation. *Lab Invest J Tech Methods Pathol.* 2008;88(11):1143–1156.
  39. Schmidinger G, Hanselmayer G, Pieh S, et al. Effect of tenascin and fibronectin on the migration of human corneal fibroblasts. *J Cataract Refract Surg.* 2003;29(2):354–360.
  40. Ljubimov AV, Atilano SR, Garner MH, Maguen E, Nesburn AB, Kenney MC. Extracellular matrix and Na<sup>+</sup>, K<sup>+</sup> - ATPase in human corneas following cataract surgery: comparison with bullous keratopathy and Fuchs' dystrophy corneas. *Cornea.* 2002;21(1):74–80.
  41. Nakagawa T, Okumura N, Ikegawa M, et al. Shotgun proteomics identification of proteins expressed in the Descemet's membrane of patients with Fuchs endothelial corneal dystrophy. *Sci Rep.* 2023;13:10401.
  42. Miyazaki K, Okada Y, Yamanaka O, et al. Corneal wound healing in an osteopontin-deficient mouse. *Invest Ophthalmol Vis Sci.* 2008;49(4):1367–1375.
  43. Sumioka T, Kitano A, Flanders KC, et al. Impaired cornea wound healing in a tenascin C-deficient mouse model. *Lab Invest.* 2013;93(2):207–217.
  44. Kothari AN, Arffa ML, Chang V, et al. Osteopontin—a master regulator of epithelial-mesenchymal transition. *J Clin Med.* 2016;5(4):1–16.
  45. Katikireddy KR, White TL, Miyajima T, et al. NQO1 down-regulation potentiates menadione-induced endothelial-mesenchymal transition during rosette formation in Fuchs endothelial corneal dystrophy. *Free Radic Biol Med.* 2018;116:19–30.
  46. Aldave AJ, Han J, Frausto RF. Genetics of the corneal endothelial dystrophies: an evidence-based review. *Clin Genet.* 2013;84(2):109–119.
  47. Malhotra D, Jung M, Fecher-Trost C, et al. Defective cell adhesion function of solute transporter, SLC4A11, in endothelial corneal dystrophies. *Hum Mol Genet.* 2020;29(1):97–116.
  48. Krachmer JH, Purcell JJ, Young CW, Bucher KD. Corneal endothelial dystrophy. A study of 64 families. *Arch Ophthalmol Chic Ill 1960.* 1978;96(11):2036–2039.
  49. Douth JJ, Quantock AJ, Joyce NC, Meek KM. Ultraviolet light transmission through the human corneal stroma is reduced in the periphery. *Biophys J.* 2012;102(6):1258–1264.
  50. Choi SI, Dadakhujaev S, Ryu H, Kim T, Kim EK. Melatonin protects against oxidative stress in granular corneal dystrophy type 2 corneal fibroblasts by mechanisms that involve membrane melatonin receptors. *J Pineal Res.* 2011;51(1):94–103.
  51. Joyce NC, Zhu CC, Harris DL. Relationship among oxidative stress, DNA damage, and proliferative capacity in human corneal endothelium. *Invest Ophthalmol Vis Sci.* 2009;50(5):2116–2122.
  52. Jurkunas UV, Bitar MS, Funaki T, Azizi B. Evidence of oxidative stress in the pathogenesis of Fuchs endothelial corneal dystrophy. *Am J Pathol.* 2010;177(5):2278–2289.

53. Xu I, Thériault M, Brunette I, Rochette PJ, Proulx S. Matrix metalloproteinases and their inhibitors in Fuchs endothelial corneal dystrophy. *Exp Eye Res.* 2021;205:108500.
54. Gottsch JD, Bowers AL, Margulies EH, et al. Serial analysis of gene expression in the corneal endothelium of Fuchs' dystrophy. *Invest Ophthalmol Vis Sci.* 2003;44(2):594–599.
55. Taylor SH, Yeung CYC, Kalson NS, et al. Matrix metalloproteinase 14 is required for fibrous tissue expansion. *eLife.* 4:e09345.
56. Zamilpa R, Lopez EF, Chiao YA, et al. Proteomic analysis identifies in vivo candidate matrix metalloproteinase-9 substrates in the left ventricle post-myocardial infarction. *Proteomics.* 2010;10(11):2214–2223.
57. Agnihotri R, Crawford HC, Haro H, Matrisian LM, Havrda MC, Liaw L. Osteopontin, a novel substrate for matrix metalloproteinase-3 (stromelysin-1) and matrix metalloproteinase-7 (matrilysin)\*. *J Biol Chem.* 2001;276(30):28261–28267.
58. Filenius S, Tervo T, Virtanen I. Production of fibronectin and tenascin isoforms and their role in the adhesion of human immortalized corneal epithelial cells. *Invest Ophthalmol Vis Sci.* 2003;44(8):3317–3325.
59. Kariya Y, Kanno M, Matsumoto-Morita K, Konno M, Yamaguchi Y, Hashimoto Y. Osteopontin O-glycosylation contributes to its phosphorylation and cell-adhesion properties. *Biochem J.* 2014;463(1):93–102.
60. Engler C, Kelliher C, Speck CL, Jun AS. Assessment of attachment factors for primary cultured human corneal endothelial cells. *Cornea.* 2009;28(9):1050–1054.
61. Rizwan M, Peh GS, Adnan K, et al. In vitro topographical model of Fuchs dystrophy for evaluation of corneal endothelial cell monolayer formation. *Adv Healthc Mater.* 2016;5(22):2896–2910.
62. Whitcher JP, Srinivasan M, Upadhyay MP. Corneal blindness: a global perspective. *Bull World Health Organ.* 2001;79(3):214–221.
63. Leask A, Abraham DJ. TGF- $\beta$  signaling and the fibrotic response. *FASEB J.* 2004;18(7):816–827.